ARTICLE

Check for updates

High-frequency chaotic bursts in laser diode with optical-feedback

Tushar Malica [1,2 ✉], Guillaume Bouchez[1,2 ✉], Delphine Wolfersberger[1,2 ✉] & Marc Sciamanna[1,2 ✉]

The diversity of observed nonlinear dynamics in laser diodes subjected to optical feedback shows promise as an excellent candidate for chaos-based commercial applications. Thus, works in the last decade have primarily focused on system performances, geometric configurations, and balancing their trade-offs. We demonstrate an optical feedback system operating on phase-conjugate feedback exhibiting state-of-the-art chaos bandwidth values reaching $\approx 30\ GHz$. We report numerous high-frequency, spatiotemporally complex, chaotic dynamics undocumented in the past four decades. We highlight the underlying physics involving a three-tier temporal interaction mechanism between laser relaxation oscillations, phase-conjugate feedback induced external cavity modes, and chaotic bursts repeating each delay time in the extended cavity. We show supporting real-time high-definition system outputs captured by modern large bandwidth oscilloscopes. The presented work shows to our knowledge, the highest bandwidth and complexity entropy to-date in an optical chaos from a single laser, thereby proving the unnecessary need for further complexity using cascading lasers.

[1] Chaire Photonique, LMOPS, CentraleSupélec, 2 Rue Edouard Belin, 57070 Metz, France. [2] Université de Lorraine, LMOPS, 2 Rue Edouard Belin, 57070 Metz, France. ✉email: tushar.malica@centralesupelec.fr; guillaume.bouchez@centralesupelec.fr; delphine.wolfersberger@centralesupelec.fr; marc.sciamanna@centralesupelec.fr

Nonlinear optical systems with delayed feedback is a configuration where the light emission from a laser source is reflected back into itself[1]. The distance between the laser source and the reflective optic comprises the external cavity length and determines the feedback delay. The laser dynamics may be destabilized (or stabilized) by explicitly controlling the interference between the forward and the backward propagating light waves using experimental parameters such as feedback strength, alignment of the reflective optic, external cavity length, bias current, and temperature.

Deviations from the linear stable behavior into the nonlinear regime is widely reported in many forms and one of the more commonly observed is the high-dimensional chaos[1–4]. The purpose of destabilizing a stable single-wavelength light source to generate chaos is ultimately for commercial uses, particularly in the field of secure optical communication and encryption[1,5–8]. Specifically for chaos-based communication applications, the key is to use high-dimensional chaos to encrypt a system while maintaining fast transmission speed.

Hence, quantifying the complexity and bandwidth of chaos in the nonlinear regime of delay systems become critical figures of merit. Chaotic laser outputs show unpredictability, i.e., the nature of laser emission at a given time 't' is independent from the nature of past outputs. This translates to an absence of characteristic timescales and frequencies in the temporal and frequency domains respectively and ideally similar to the case of white gaussian noise.

In real-life optical delay systems, the timescale associated with the delay, in addition to the relaxation oscillation frequency are always known to be present to regulate all nonlinear mechanisms. Of the many choices available, phase inverted wave-fronts when reflected into its semiconductor laser source by an external reflector is a commonly known experimental technique to observe phase-conjugated feedback (PCF)[9–18]. Such a system has an inherent predisposition to lock onto an integral multiple (N) of the external cavity frequency f_{cav} which is equivalent to the reciprocal of the external cavity round-trip time ($1/\tau_{RT}$). This PCF-specific property exhibits harmonic solutions known as the external cavity modes (ECMs) that pulsate at a frequency many times higher than the external cavity frequency, i.e., $f_{ECM} = N f_{cav}$[14,17].

These ECMs have been shown and extensively analyzed theoretically[9–14,19,20] and only recently discovered experimentally[21]. Consequently, the predictability of the observed ECMs is high due to the periodicity despite the numerous overlaying timescales modulating the ECMs in amplitude[18]. Furthermore, theoretical works such as[9] initially explained the self-pulsations as undamped relaxation oscillations leading to chaos which was later experimentally disproved in refs.[16,22]. However, till-date the origin of such high values of reported chaos bandwidth (30 GHz $>> f_{RO}$ in the presented work) is unexplained.

Furthermore, it has been established that the performance of PCF systems in terms of chaos bandwidth surpasses alternative optical-feedback systems (OFS). Our recent work shows the system exhibits a consistently high chaos bandwidth (up to ~30 GHz) independent of the feedback strength[17,18,23]. In particular, the analysis made in ref.[16] shows that the wide-band chaos in the PCF systems has a bandwidth up to 27% larger than the one exhibited by a conventional optical-feedback (COF) system where one uses a simple mirror as the external reflector. In addition, the general predictability across the parameter space defined by the feedback strength is significantly higher for the case of COF system when compared to its PCF counterpart[18,24]. Hence, the PCF system is a better choice among single optical-feedback configurations to generate high-dimensional chaos from a signal-based perspective of chaos performance. One may further complexify the experimental setup and employ multiple lasers in an attempt to boost system performance in terms of chaos bandwidth such as in refs.[5,25–27]. However, the trade-off hampers its commercial viability and the performance is either inferior by 50% as in refs.[5,25,27] to the presented work, or, surpasses at most by merely 8 GHz as in refs.[26].

From the perspective of differential-delay systems exhibiting irregular chaotic dynamics, typically two temporal signatures corresponding to the relaxation oscillation time (τ_{RO}) and the τ_{RT} are known to regulate the system[28]. This results in chaotic oscillations which are nonlinearly mixed with the aforementioned two characteristic timescales and may further be interrupted by bursts of pulses that repeat on a much slower timescale. Examples of such dynamics commonly observed to-date include synchronous low-frequency fluctuations (LFF) in long external cavity OFS ($\tau_{RT} > \tau_{RO}$)[29,30], regular pulse packages in the short external cavity OFS ($\tau_{RO} > \tau_{RT}$)[31,32], and chaotic breathers which repeat at a slow frequency of the bandpass filter in optoelectronic feedback[4].

Given the massive theoretical analysis reported since the 90s, we focus our work towards the experiments that are now possible to capture previously unseen features of the dynamics with state-of-the-art high-resolution oscilloscopes. This experimental work captures and investigates the singular dynamical events whose presence pushes the upper limit of chaos bandwidth by several gigahertz. Not to overlook that the system has shown spatiotemporal self-rearrangement at a dynamical state while maintaining its complexity in the chaotic regime[18]. The system is proven to be driven by a sophisticated interplay between regular and complex dynamical processes which is to-date unexplored and is thus, the topic of the presented research. The presented work is motivated by the experimental observations in ref.[18] that the system under consideration is primarily designed to generate regular ECM dynamics but counterintuitively capable of exhibiting extremely high values of chaos bandwidth upon applying high feedback strength and whose origin is presently unknown. While investigating the origin of the superior chaos performance of the presented PCF system, we uncover previously undocumented three-timescale dynamics where the internal regular dynamics occurs at a significantly faster timescale than the chaos. Destabilized ECM dynamics pulsating at a superharmonic of the ECM are interrupted by the chaotic bursts that are much slower having a periodicity of the round-trip time. In contrast to the dynamics reported in the past 50 years, these chaotic bursts are not induced by an external timescale[28–32] or the filter bandwidth as in ref.[4] but by the delay itself. As a result and also contrary to LFF, the repetitive rate of the bursts is also independent of the bias current. Therefore, we also demonstrate the many layers of timescales interplaying along the spatiotemporal domain that makes a PCF system complex. Commonly known mechanisms that create deterministic chaos in other optical-feedback systems do not support these observations and thus, need to be addressed.

Results and discussion

The following section shows four dynamical outputs observed in the high feedback region when $\eta > 3\%$. It should be noted that this region of parameters displays erratic switching of dynamics between periodic and complex dynamics with no regular trend as a function of feedback strength. Multistability between ECMs and chaos, and between ECMs themselves has indeed been predicted theoretically when increasing the feedback strength as a consequence of the close proximity of Hopf bifurcations yielding ECMs solutions[20,33]. Therefore, we focus on the qualitative nature of the observed dynamics and classify them into four
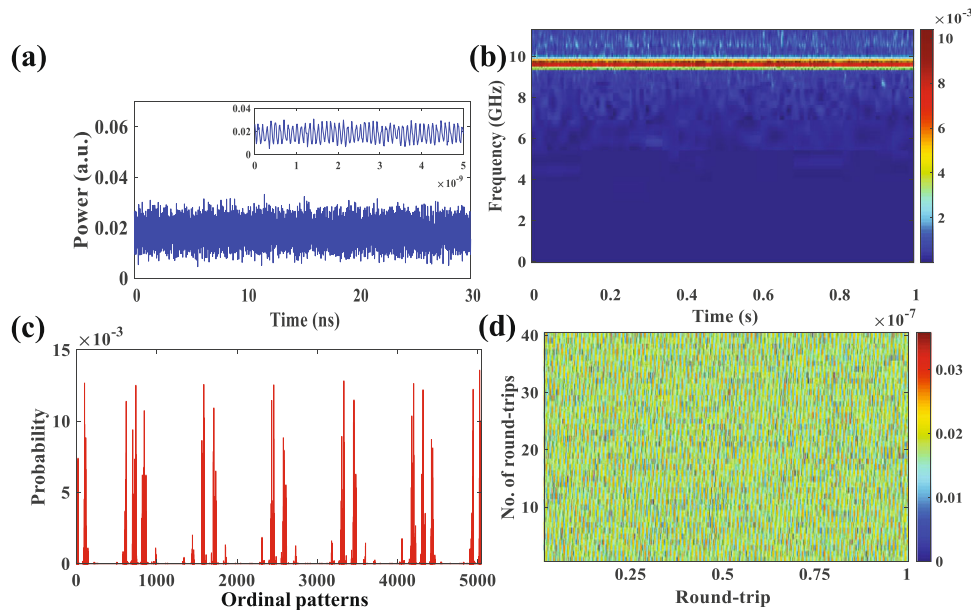
Fig. 1 Stable external cavity modes (ECMs). a System output in the temporal domain with the inset showing a 5 ns subset. **b** Time localization of the spectral components in the Fourier domain for a 100 ns long sample. Color bar shows the frequency energy amplitude. **c** Ordinal pattern preference using ordinal pattern length (D) = 7 and length of time-series (N) = 36×10^3. **d** System output in the spatiotemporal domain where the horizontal axis represents changes over a single round trip while the vertical axis show changes observed over multiple round-trips. Color bar shows the signal amplitude. Presented example acquired at feedback strength (η) = 3.38%, repetition rate (f_{rep}) = 30 GHz, and ECM frequency (f_{ECM}) = 9.81 GHz = $101 f_{cav}$, where, f_{cav} is the external cavity frequency.

behaviors that are arranged from the most stable and periodic to chaotic outputs in the following text.

External cavity modes and their destabilization. Figure 1 shows the case for stable ECMs in temporal, frequency and complexity domain respectively. As briefly defined before, ECMs are time-periodic pulsations, as shown in the inset of Fig. 1a. They have a repetition rate (f_{ECM}) of ~10 GHz as shown using continuous wavelet transform (CWT) in Fig. 1b. The complexity of this dynamical state arises from the additional existing timescales that modulate the periodic pulsations in amplitude, and amplitude and timing jitter of the pulses. Figure 1c shows the probability of occurrence of a given ordinal pattern. All 5040 of the possible ordinal patterns are indicated by the horizontal axis. The vertical axis shows the probability of each pattern. A stable ECM has a strong and clear preference to very specific ordinal patterns. This is because the exhibited dynamical state is dominated by periodic pulses resulting in the increased predictability, thereby, lowering the permutation entropy (PE) represented by $\rho_{RT} \approx 0.65$. The spatiotemporal representation shows ECMs comprising ~100 pulses in one external cavity round trip as shown in Fig. 1d. The variation in colorscale shows the variation in amplitude of pulses as shown in the inset of Fig. 1a.

Increased feedback strength destabilizes the ECM as shown in Fig. 2a. The destabilization via quasi-periodicity as shown in Fig. 2b shows the presence of additional nearby frequencies gaining prominence. This is also evident from Fig. 2d as one-dimensional striations are seen in the spatial domain. The preference of ordinal patterns remains largely the same as Fig. 2c since the global nature of the dynamical state remains unchanged with a slight drop in the probability of the most favored ordinal patterns. Simultaneously, the probability of the subgroups of the ordinal patterns in immediate surrounding will increase as well.

Chaos and the mixed dynamics. Figure 3a shows the case for an intermediate chaotic state systematically switching between ECMs

and wide-band chaos. Note the changing scale of frequencies exhibited has significantly increased as seen in Fig. 3b. Presented dynamics have not been experimentally acquired and reported at such high resolution in comparable OFSs, to the best of our knowledge. The wide-band chaos originates from the high power bursts spaced round-trip time apart consistently as shown in Fig. 3a and d. The duration of the event is observed to steadily increase at an average rate of 60 ps per round trip. These bursts are extremely chaotic in nature with a wide range of frequencies (2.5–35 GHz) as seen in Fig. 3b with frequencies higher than 20 GHz having the most power and the observed turbulence extends across the spatial domain as seen in Fig. 3d. The chaotic bursts always begin with a power dropout analogous to those previously reported in refs. [15,34]. The system recovery is accompanied by deterministic high-dimensional chaos during the entire duration of a chaotic burst as shown by Fig. 3b. This is followed by the non-chaotic low-amplitude signal observed for the remainder of the round trip. The corresponding frequencies are fractional multiples of f_{ECM} such as ≈ 0.6, 2.5, 5, and 10 GHz. Moreover, the chaotic bursts build from these lower frequencies as well. One can say that this dynamical state is characterized by suppressed and attenuated ECMs bounded by chaotic bursts. As seen in Fig. 3c, the presence of chaotic bursts results in high unpredictability and overall complexity ($\rho_{RT} > 0.96$) suggests a true deterministic chaotic state. There is no preference to any specific ordinal patterns. Thus, the non-stationary nature of the switching dynamics means that the chaotic bursts contribute towards complexity substantially more than the attenuated non-chaotic ECMs.

The absence of the aforementioned dynamical switching results in another chaotic state as shown in Fig. 4a . The chaotic turbulence invades both the temporal and spatial domain completely as seen in Fig. 4d. The spectral distribution in Fig. 4b is not only wide range in terms of frequencies at a given instant of time, but, is inconsistent and random across the observed time sample. The chaotic nature is confirmed in Figs. 4c, d. Comparing
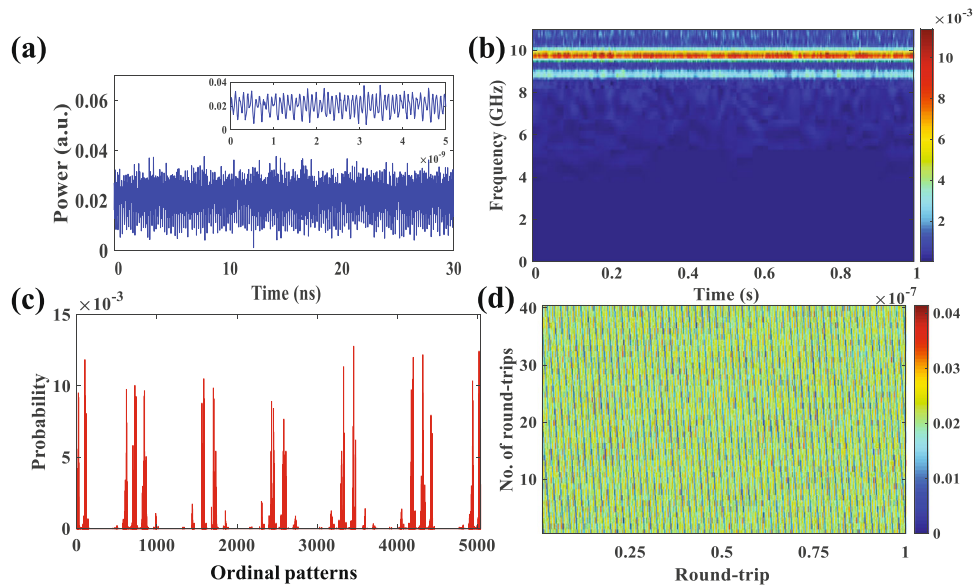
Fig. 2 Semi-stable external cavity modes (ECMs) with period-doubling. a System output in the temporal domain with the inset showing a 5 ns subset. **b** Time localization of the spectral components in the Fourier domain for a 100 ns long sample. Color bar shows the frequency energy amplitude. **c** Ordinal pattern preference using ordinal pattern length (D) = 7 and length of time-series (N) = 36 × 10³. **d** System output in the spatiotemporal domain where the horizontal axis represents changes over a single round trip while the vertical axis show changes observed over multiple round-trips. Color bar shows the signal amplitude. Presented example acquired at feedback strength (η) = 3.96%, repetition rate (f_{rep}) = 30 GHz, and ECM frequency (f_{ECM}) = 10.69 GHz ≈ 101f_{cav}, where, f_{cav} is the external cavity frequency.
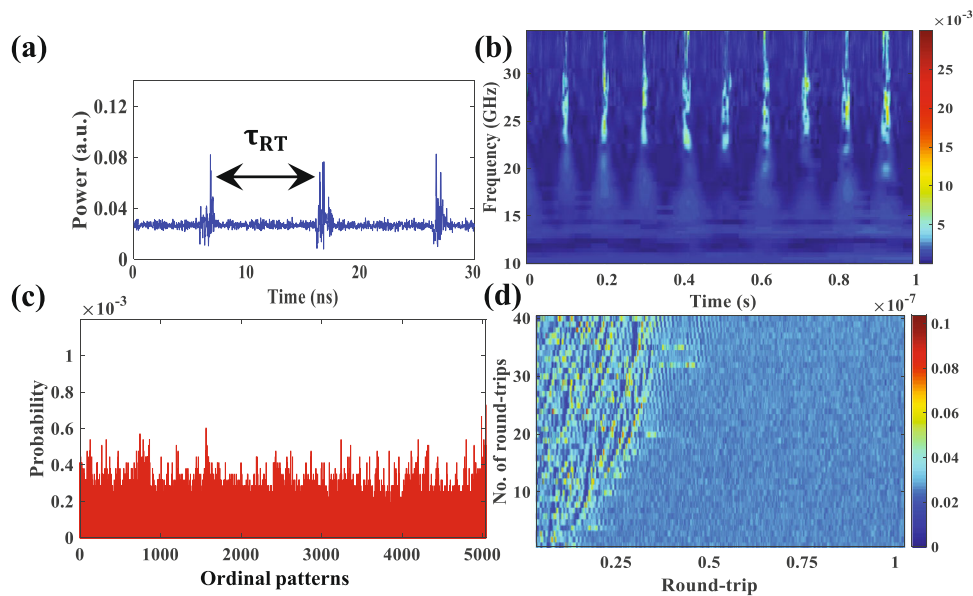

Fig. 3 Intermediate chaotic state with wide-band chaotic bursts. a System output in the temporal domain with two adjacent chaotic bursts consistently being external cavity round-trip time (τ_{RT}) apart. **b** Time localization of the spectral components in the Fourier domain for a 100 ns long sample. Color bar shows the frequency energy amplitude. **c** Ordinal pattern preference using ordinal pattern length (D) = 7 and length of time-series (N) = 36 × 10³. **d** System output in the spatiotemporal domain where the horizontal axis represents changes over a single round trip while the vertical axis show changes observed over multiple round-trips. Color bar shows the signal amplitude. Presented example acquired at feedback strength (η) = 3.37% with chaos bandwidth (β) = 26.89 GHz.

Fig. 3c to Fig. 4c, one can see that the dynamical state shown in Fig. 4c has a proclivity to favor fewer ordinal patterns compared to the situation observed in Fig. 3c. This might seem counter-intuitive based solely on observations based on the spatiotemporal domain i.e., Figs. 3d and 4d, thereby, highlighting the importance of CWT and plots showing probability distribution of the ordinal patterns for non-stationary dynamical states. We infer that the chaotic bursts are far more complex and chaotic than the

case of the chaotic state. It should be noted that this is not apparent on comparing the normalized complexity values solely, which remains similar for both the states being highly chaotic with $\rho_{RT} > 0.94$ and similar chaos bandwidth ($\beta \approx 26$ GHz). However, this does impact the spectral flatness of the RF spectrum with the spectral flatness for Fig. 3c being of higher value than for Fig. 4c. Therefore, an operating condition purely consisting of chaotic bursts as shown in Fig. 3a confirms that such
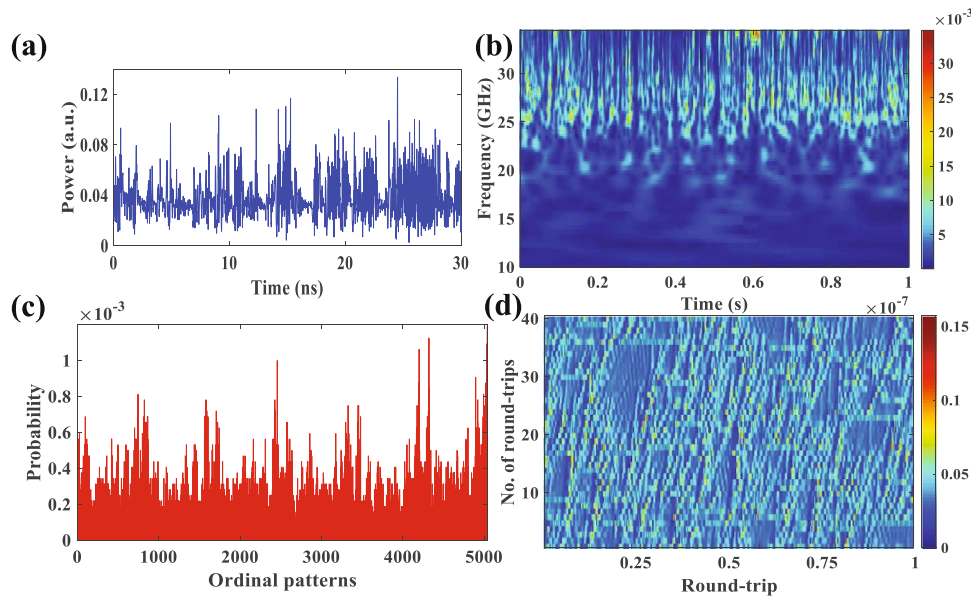
Fig. 4 Chaotic dynamical state. a System output in the temporal domain. **b** Time localization of the spectral components in the Fourier domain for a 100 ns long sample. Color bar shows the frequency energy amplitude. **c** Ordinal pattern preference using ordinal pattern length (D) = 7 and length of time-series (N) = 36×10^3. **d** System output in the spatiotemporal domain where the horizontal axis represents changes over a single round trip while the vertical axis show changes observed over multiple round-trips. Color bar shows the signal amplitude. Presented example acquired at feedback strength (η) = 3.57% with chaos bandwidth (β) = 26.9 GHz.

events contribute towards chaos while negligibly impacting spectral flatness and raising the entire spectral floor. The operating condition will exhibit weak spectral selectivity in the presence of the aforementioned chaotic bursts which directly contribute to wide-band chaos. The extent of spectral selection, and therefore, an increase in predictability of a dynamical state, will depend on the number of chaotic events. Finally, the chaos bandwidth will drop as low as 11 GHz in complete absence of the observed chaotic bursts. Consequentially, such chaotic burst dynamics emerging from destabilized ECMs, if well-controlled, may be applied for applications such as random-bit-generation and lidar sensing applications[5,7,8] since one can control the time duration (τ_{RT}) between the chaotic bursts.

The system pushes the limit of the chaos bandwidth further for the chaotic states (mixed or otherwise) through structured high-frequency random events as shown in Fig. 5a, b. An example of a single event is highlighted in red and magnified further in Fig. 5c–e. The spatiotemporal representation is shown in Fig. 5f with red arrows indicating the round trip at which the structured high-frequency random event occurs. It should be noted that the dynamical variation across the temporal domain changes erratically as opposed to Figs. 3d and 4d where the dynamics evolved spatially periodically. The chaos bandwidth can drop as low as 17–20 GHz in the absence of such events. On the other hand, increased occurrence of these events will extend the chaos bandwidth up to 35 GHz. A sample of the structured and regular signal spiking bounded by a chaotic burst in the temporal domain is shown in Fig. 5e. Figure 5b and d shows that the corresponding spectral contribution is at ≈ 35 GHz corresponding to the repetition rate of the structured signal spiking and it is restricted to a limited frequency range of ~2 GHz. The system shifts the frequency signature linearly from ~32 GHz towards the upper limit of ~35 GHz and back systematically at a frequency of ~10 GHz, i.e., the f_{ECM} during this event. An additional timescale corresponding to the amplitude modulation is observed at ~5 GHz ≈ f_{ECM}/2. All these evidences suggest that the structured high-frequency random events are driving the system to exhibit ECMs at a frequency much higher than the typical stable case

observed in Figs. 1 and 2. However, these events are short-lived indicating that the system is not able to sustain ECMs at frequencies higher than currently observed over extended period of time. The time duration of these events is at most the length of the round-trip time but may be shorter in intermediate and mixed dynamical states. They are observed to be always triggered and end with a chaotic burst dynamically. It may be argued that such events have evolved from switched dynamical state observed in Fig. 3a but with amplified ECMs bounded between chaotic bursts. The signal energy during the sub-event of amplified ECMs is split between two sets of frequencies, i.e., ~25 GHz and ~35 GHz as seen in Fig. 5c. However, the observed energy redistribution is not always split with the higher frequency always present. Therefore, the system inherently pushes the limit of the measured chaos bandwidth through spatiotemporally ordered and well-structured events.

One also observes the dynamics transition between a chaotic burst event and a structured high-frequency random event over a round trip at a single operating condition as seen in Fig. 6. The system begins at a state similar to the case seen Fig. 3d with turbulence creeping in solely in the spatial domain. The system evolves as time elapses and the dynamical variation is observed both in the spatial and temporal domain. The system self-organizes to exhibit islands of regular dynamics bounded by turbulence and chaotic bursts at later round-trips (>20). Change in complexity and chaos bandwidth is insignificant; however, system shows control and the ability to switch back and forth between complex dynamical states within a round trip. To-date such structured high-frequency random events and wide-band chaotic bursts have not been reported for the COF systems to the best of our knowledge. However as seen during chaotic mixed states, one similarity with the COF systems is the system's inclination to take the route of exhibiting low-frequency dynamics (similar to the well-documented low-frequency fluctuations in the COF systems) prior to its transition to chaos.

It can further be inferred that the observed frequency description is inherent to the system as there is no correlation to the feedback strength, applied current or other experimental
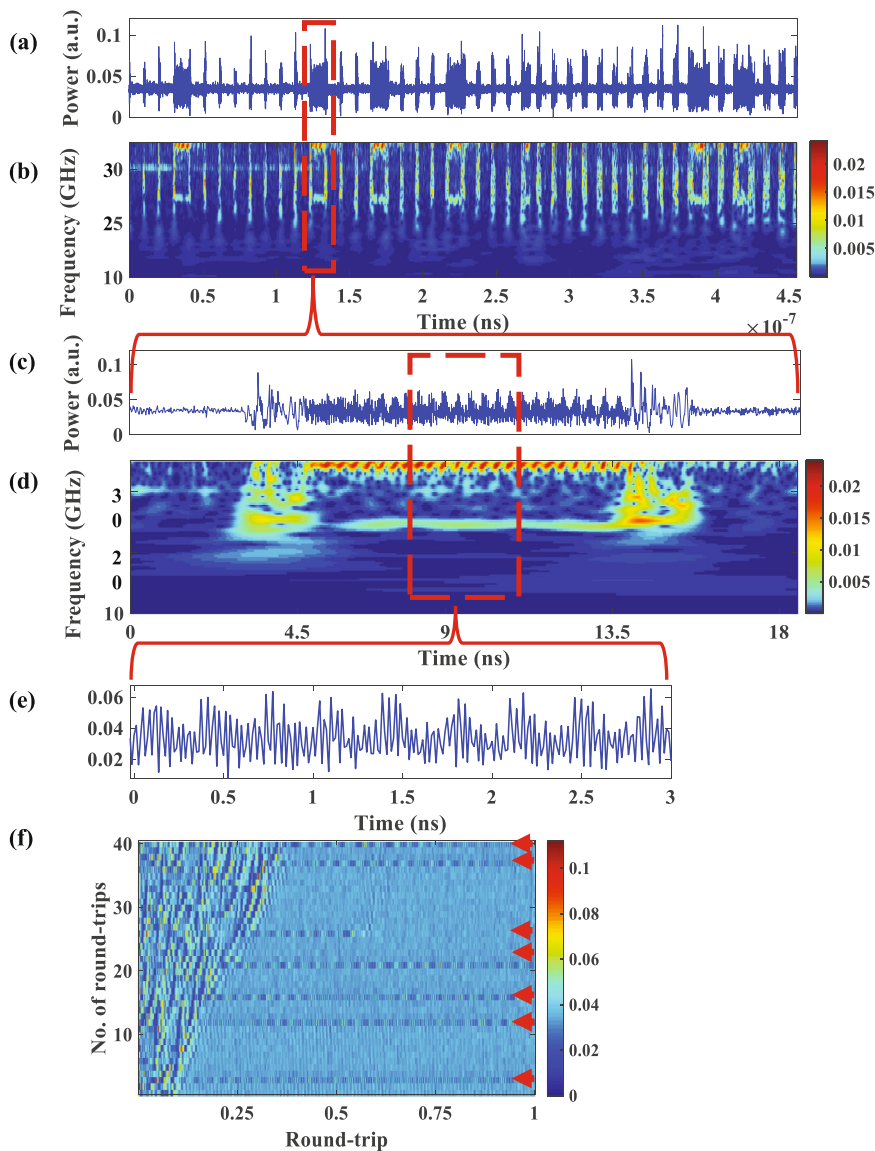
Fig. 5 Mixed dynamical state with high-frequency random events. a A sample of time-series in the temporal domain. **b** Time localization of the spectral components in the Fourier domain for a 100 ns long sample. Color bar shows the frequency energy amplitude. **c** Structured high-frequency random event shown in detail. **d** A magnified subset of the event showing contents of the high-frequency event. **e** Amplitude modulation observed with a carrier frequency of 30 GHz. The upper and lower sideband frequencies are 3 GHz apart from the carrier frequency. **f** Shows the system output in the spatiotemporal domain where the horizontal axis represents changes over a single round trip while the vertical axis show changes observed over multiple round-trips. Color bar shows the signal amplitude. The high-frequency events are indicated by red arrows. Presented example acquired at feedback strength $(\eta) = 3.07\%$ with chaos bandwidth $(\beta) = 30.23$ GHz.

parameters to the duration, presence, or frequency of the events at an operating condition. This is shown in Fig. 7 through a variety of mixed dynamics comprising of the events described up to this point. Figure 7a–c shows the case of a long round-trip time i.e., 10.3 ns. Figure 7d–f shows the case of a short round-trip time i.e., 3.55 ns. Note that the figure shows same number of round-trips for fair comparison.The upper limit of the exhibited frequency of ~35 GHz observed is independent of the round-trip time. A change in round-trip time has experimentally confirmed a change in the maximum allowable duration of the structured high-frequency random event. The difference, however, lies in presence of the lower frequency related to f_{ECM} which are absent for the short round trip, i.e., Fig. 7d–f. The system's ability to exhibit stable ECMs, regardless of the signal amplitude, is essentially absent in the case of short round-trip time. This may

be due to the limitation of time available inside the external cavity for proper stabilization of such dynamics. Additionally, by increasing the current from Fig. 7d–f, the frequency spread in CWT becomes more diverse as current increases. The wide-band chaotic burst events are weak at lower currents.

Agreement with theory. On simulating this PCF system with an external cavity round-trip time (τ) of 10.3 ns and parameters ($P = 0.606$, $T = 1200$, $\alpha = 3$, $\tau_p = 2ps$, $\tau_R = 50$, $R = 10^{-12}$), we confirm existence of dynamics as seen in Figs. 1, 2, and 4. However, the current theoretical model does not predict the chaotic bursts occuring periodically at round-trip time experimentally as observed in Fig. 3. The presence or absence of weak COF and noise does not change the observations qualitatively.

Extensive simulations have been performed varying the phase-conjugate nirror penetration ($\tau_R = 50$), adding parasitic COF $\gamma' = 0.1$ and $\tau = 10.3$ ns, or additional noise but without success. The exact physical mechanism at the origin of the chaotic bursts shown in Figs. 3a, b remains, therefore, unclear. Since PCF simulations exclude the impact of the filter bandwidth, noise, or parasitic COF effects, a mechanism involving multistability and intermittent but periodic switching between destabilized ECMs remains the most probable mechanism in place here.

Conclusions

Previously unreported three-timescale regulating laser diode dynamics subjected to optical feedback is demonstrated in the form of chaotic bursts. These chaotic oscillations born on limit cycles with frequency signatures corresponding to the super-harmonic multiples of the external cavity frequency are interrupted by chaotic bursts of even much higher frequencies that repeat every round-trip time in the external cavity. These delay-
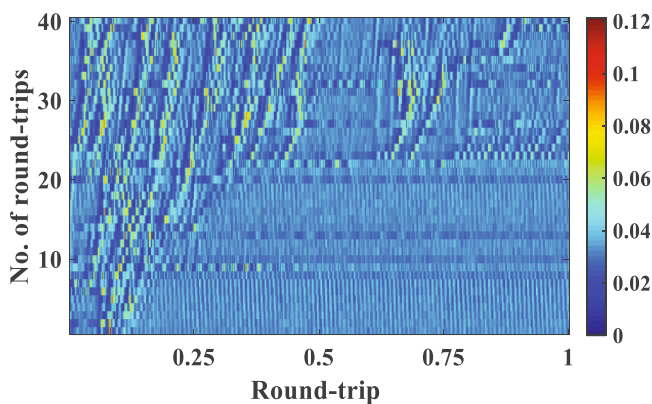

Fig. 6 Transitional mixed dynamical state. Transitional state between Fig. 4 and Fig. 5. System output in the spatiotemporal domain where the horizontal axis represents changes over a single round trip while the vertical axis show changes observed over multiple round-trips. Color bar shows the signal amplitude. Presented example acquired at feedback strength (η) = 3.98% with chaos bandwidth (β) = 26.2 GHz.

repetitive chaotic bursts explain the much superior performances of the chaos generated over the chaos generated from a more conventional optical-feedback system. High-dimensional deterministic chaos and multi-layered spatiotemporal complexity are indicated as the system exhibits a chaotic bandwidth of over 30 GHz and a permutation entropy up to 0.99 over a wide range of experimental parameters. This discovered dynamics benefits the rising stream of generic application of chaos from a laser diode.

The path of an ECM towards chaos is explored and the distinct dynamics contributing towards chaos bandwidth and destabilized ECMs are captured. Different dynamical states are identified through qualitative analysis in the temporal, frequency and complexity domains. The genesis of chaos is explained through exploration of the isolated dynamical events that push the limit of chaos bandwidth while maintaining the spatiotemporal complexity. These dynamics are observed to be regulated at a much slower timescale than the internal dynamics, thereby, making the PCF system a three-timescale optical delay system. It is shown that the upper limit of the chaos bandwidth is intrinsic to the system and independent of the round-trip time. An increase in the bias current contributes towards the generation of a higher number of the identified chaotic dynamical events but in a random manner. A variation of feedback strength is shown to control the destabilization of the ECMs and take the system towards chaotic states. The presented system is shown to exhibit state-of-the-art limit of chaos bandwidth of up to 35 GHz and the performance is significantly better than a COFS counterpart. Additionally, the entire parameter space is observed to be spatiotemporally extremely complex indicated by the permutation entropy analysis.

The system's multidimensionality comes forth as it shows ability to switch between time-stationary and non-stationary states. On a global level, all dynamically chaotic states exhibit high chaos bandwidth and complexity with insignificant changes that restrict their differentiation and classification, if solely based on the face value of the aforementioned figures of merit. However, exploration of the spread of ordinal patterns at a dynamical state and contribution of frequencies at an instant of time, together, provides clarity on the nature and extent of chaos observed. It is stressed here that the experimentally captured dynamical events
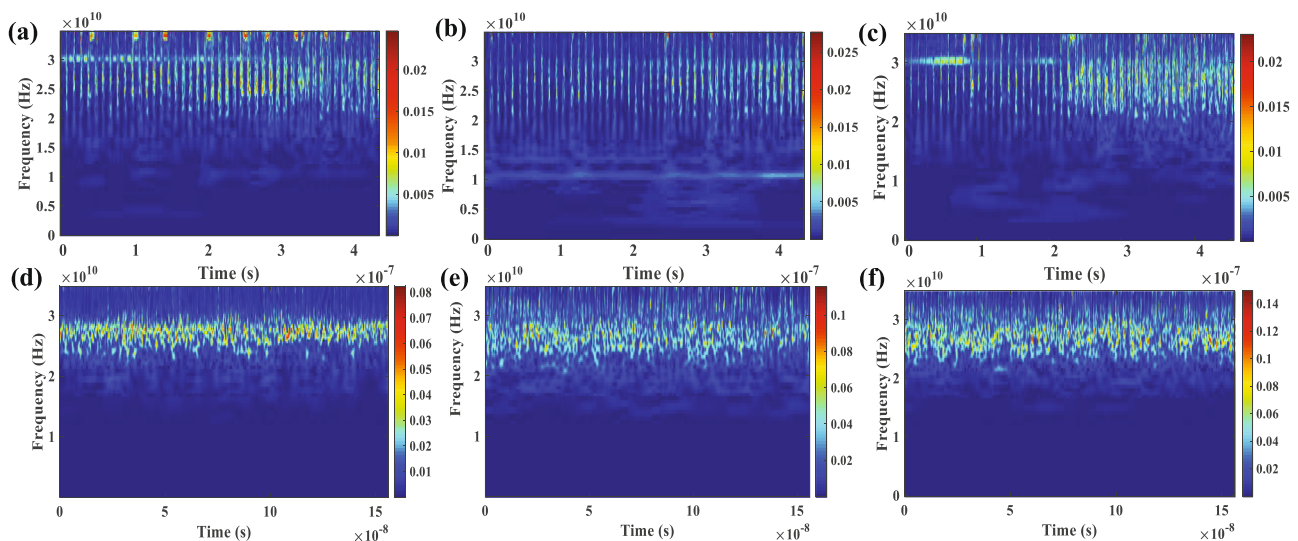

Fig. 7 Mixed dynamics with high spatiotemporal complexity observed over 45 round-trips at different round-trip times (τ_{RT}). a–c Acquired at $\tau_{RT} = 10.3$ ns and $I = 80$ mA showing independence to the feedback strength with **a** $\eta = 2.77\%$, $\beta = 28.76$ GHz, **b** $\eta = 3.29\%$, $\beta = 28.19$ GHz, and **c** $\eta = 3.98\%$, $\beta = 26.21$ GHz. **d–f** Acquired at $\tau_{RT} = 3.55$ ns and $\eta = 2.5\%$ showing independence to the current applied for **d** $I = 40$ mA, **e** $I = 60$ mA, and **f** $I = 80$ mA. The color bars represent frequency energy amplitude. Normalized permutation entropy (ρ_{RT}) > 0.9 for all cases. η: feedback strength, β: chaos bandwidth, and I: applied current.
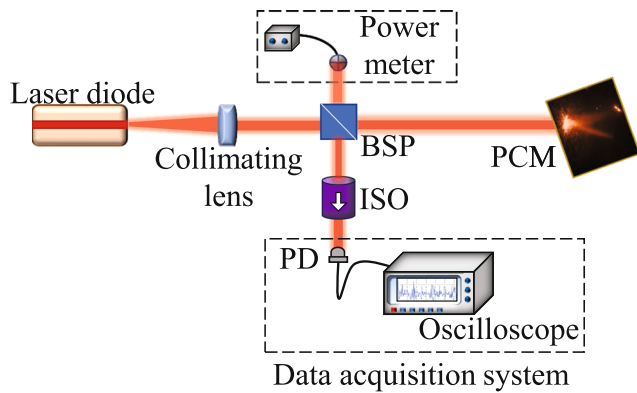
Fig. 8 Experimental setup showing an 852 nm laser diode subjected to PCF using a BaTiO₃ crystal. The external cavity round-trip time ≃ 10.3 ns. BSP beam splitting plate, PCM phase-conjugate mirror, ISO Faraday isolator, PD photodiode.

regulated by three distinct timescales have not been documented or observed for a delayed optical system to the best of our knowledge. Additionally, the capability of the system to vary the dynamics at an operating condition between chaotic and pulsed-states systematically over extended period of time is reported. On the other hand, the system also can switch between chaotic and pulsed-states over a single round trip. This unique property of the PCF system where duality in dynamics resides at a single operating condition makes for a rich system that may be controlled and specifically explored for high-speed chaos-based applications.

Methods

Experimental setup. The experimental setup as shown in Fig. 8 uses a commercial Fabry-Pérot semiconductor laser (JDS Uniphase DL-SDL-5420) with a threshold current of 14.9 mA and an emission wavelength of 852 nm. The laser diode operates within the current range of 20–130 mA. The system is maintained at an operating current of 80 mA and a temperature of 20 °C. The collimating lens is an aspheric objective lens (Newport 5722-B-H) with an effective focal length of 4.5 mm. A 80:20 beam splitting plate (BSP) is used to split laser emission in three different directions. PCF is generated using a Rh-doped BaTiO₃ photorefractive crystal (5 × 5 × 5 mm) from the incoming laser emission transmitted through the BSP. The incoming light is known to fan out at the air-crystal interface due to the beam coupling between the forward propagating incident waves and the scattered waves caused by the inhomogeneous crystal. As the deviated light traverses through the crystal, it experiences total internal reflection on the different facets of the bulk crystal. Such reflected beams interact among themselves resulting in a phase-conjugated backwards propagating laser beam due to the phenomenon of four-wave mixing[35]. The system output is coupled into a standard monomode fiber carrying it into a 38 GHz BW photodiode (Newport 1474-A). The free-space optical isolator (Thorlabs IO-3-850-HP) prevents the reflections from the coupler. An oscilloscope (Teledyne LeCroy 10-Zi-A 36 GHz) is used to record system outputs as digitized time-series at a sample rate of 80 GS/s. It should be noted that in spite of the data acquisition system comprising the photo-receiver and the oscilloscope being state-of-the-art at 850 nm, the reported chaos bandwidth is close to the bandwidth limit of the signal acquisition system and its exact value may be higher by 2–4 GHz. However, the qualitative nature of the system output and thus, the dynamical nature of the reported study will remain unchanged. 20% of the laser emission from the BSP is fed to a power meter for acquiring the feedback value. The external cavity round-trip time (T_{RT}) is ≃ 10.3 ns with a corresponding cavity length equivalent to ≃ 1.545 m and an external cavity frequency of ≃ 97.09 MHz unless specified otherwise.

Permutation entropy (PE). We quantify complexity using a concept from information theory, developed by Bandt and Pompe[36], known as permutation entropy. The algorithm measures the predictability of the recurring temporal patterns in a time-series. This is done by comparing the relative magnitude of the subset data. Next, the probability distribution of the user-defined subsets of the time-series is calculated. The algorithm has been shown to be robust to non-linearity and has decent computational speed to make this our choice for complexity analysis[36,37]. Additionally, it has demonstrated application in a wide range of applications such as semiconductor laser systems[18,24,38], biomedicine[39] and the

finance sector[40]. The algorithm is detailed in refs. [36,37] and summarized in the following text.

We consider three user-defined parameters, i.e., the delay (τ), length of the time-series (N) and ordinal pattern length (D). The delay value is calculated as the ratio of the timescale of interest to the sampling time (t_{samp}). It is chosen in accordance to the timescales at which the temporal order needs to be observed. The recommended conditions that allows a good trade between complexity quantification and computational speed are $3 \leq D \leq 7$ and $N >> D$[37]. The significantly higher length of the time-series relative to the ordinal pattern length enables PE to construct large sample space containing subsets of the time-series, known as the ordinal pattern sets (Δ). Thus, the ordinal pattern length is the number of data points extracted from a time-series with each data point τ apart. Mathematically, one may construct at most $D!$ number of ordinal patterns. The normalized PE (ρ_τ) for a given probability distribution -'p' associated with -'i' integral number of ordinal patterns is therefore given by:

$$\rho_\tau = \frac{-1}{ln(D!)} \sum_{i=1}^{D!} p(\Delta_i) ln[p(\Delta_i)] \qquad (1)$$

where $0 \leq \rho_\tau \leq 1$ with zero signifying complete predictability while one indicates complete stochasticity.

In the presented study, values associated with the timescale corresponding to the external cavity round-trip time ($T_{RT} \simeq 10.3$ ns) referred to as the round-trip delay ($\tau_{RT} = 824$) will be a major timescale of interest[1,24]. High resolution is ensured by choosing $D = 7$, $N = 36404$, $1\tau = t_{samp} = 12.5$ ps [37]. Therefore, 36,404 data points are grouped in 7! or 5040 different ordinal patterns that are T_{RT} apart from each other to calculate complexity.

Continuous wavelet transform (CWT). The CWT is employed in this work to analyze a system output's contributing frequencies at a given instant of time. Typically, system outputs in the Fourier domain are represented using Fourier transform (FT) which shows the cumulative frequency signatures of a signal irrespective of the time of occurrence. The time of occurrence is meaningless to the stationary system outputs, thereby, making FT relevant. However, the system under consideration exhibits non-stationary and chaotic outputs. Therefore, time localization of the contributing frequency components is relevant to this work. Hence, CWT is used to show the time-frequency representation of the signal. Previous studies have used CWT with the chosen wavelet for analysis of chaotic data e.g., ECG, turbulent chaos, rogue waves[41–43]. We use 2D colormaps with frequency and time as the axes to show the spread of frequency components at a given instant of time to differentiate the exhibited dynamical states. In this technique, a carefully chosen wavelet sample is shifted and compressed systematically at various scales (representing frequency) and positions (representing time). It is then superimposed upon the digitized system output under test to reveal the quality of superimposition. Presented work uses the commonly used morse wavelet which resembles a sinusoidal signal modulated in amplitude and simulates a stable ECM[41]. Note that CWT simply shows the contributing frequency at a given time instant independent of the nature of the past or future data. Hence, it does not concern itself with co-existing timescales such a low-frequency modulations. It is therefore for this reason PE is used in conjunction with CWT as PE will reveal the aforementioned slower co-existing timescales of interest. The quality of super-imposition in the presented results will show the process of destabilization of an ECM when the system progresses towards chaos.

Chaos bandwidth (β). The chaos BW is a commonly used tool in optical-feedback systems such as COF, and PCF systems. It is defined as the upper limit frequency of the RF spectrum containing 80% of the signal energy[44].

Theoretical model. The experimental system is simulated using the Lang-Kobayashi model modified for phase-conjugate feedback as described in[17,45,46].

$$\dot{E}(t) = (1 + i\alpha)E(t)N(t) + \gamma E^*_{(filtered)}(t - \tau) \qquad (2)$$

$$T\dot{N}(t) = P - N(t) + (1 + 2N(t))|E(t)|^2 \qquad (3)$$

$$\tau_R E^*_{(filtered)}(t - \tau) = E^*_{(filtered)}(t - \tau) - F(t) \qquad (4)$$

where $E(t)$ is the complex normalized electric field of the laser and $N(t)$ is the real normalized carrier density at a given instant of time t. The complex normalized feedback field is denoted as $E^*_{(filtered)}(t - \tau)$ where $\tau = 10.3$ ns is the round-trip time in the external cavity. The pump parameter is denoted by $P = 0.606$, the electron lifetime by $T = 1200$, the dimensionless feedback strength by γ, and the linewidth enhancement factor is $\alpha = 3$. All times are scaled as multiples of photon lifetime, $\tau_p = 2$ ps. No phase shift is accounted in these equations since the phase shifts in the forward and backward propagating waves cancel each other[9]. A finite-depth penetration time, $\tau_R = 50$, is added to incorporate the time taken by the phase-conjugate mirrors to generate phase-conjugated beams since this is not an instantaneous event[46,47]. Additionally, one may also get some weak conventional optical feedback in real-life experimental system effects. This is incorporated by adding a parasitic term by $\gamma' E(t - \tau)$ in eqn.(2) where $\gamma' << 1$. Furthermore, noise

may be accounted using an additional term, $R\epsilon$, as the gaussian white noise (ϵ) with standard deviation of $R = 10^{-12}$.

Data availability

References

1. Sciamanna, M. & Shore, K. A. Physics and applications of laser diode chaos. *Nat. Photonics* **9**, 151–162 (2015).
2. Soriano, M. C., Garcia-Ojalvo, J., Mirasso, C. R. & Fischer, I. Complex photonics: dynamics and applications of delay-coupled semiconductors lasers. *Rev. Mod. Phys.* **85**, 421 (2013).
3. Larger, L., Penkovsky, B. & Maistrenko, Y. Laser chimeras as a paradigm for multistable patterns in complex systems. *Nat. Commun.* **6**, 1–7 (2015).
4. Kouomou, Y. C., Colet, P., Larger, L. & Gastaud, N. Chaotic breathers in delayed electro-optical systems. *Phys. Rev. Lett.* **95**, 203903 (2005).
5. Sakuraba, R., Iwakawa, K., Kanno, K. & Uchida, A. Tb/s physical random bit generation with bandwidth-enhanced chaos in three-cascaded semiconductor lasers. *Opt. Express* **23**, 1470–1490 (2015).
6. Argyris, A. et al. Chaos-based communications at high bit rates using commercial fibre-optic links. *Nature* **438**, 343–346 (2005).
7. Cheng, C.-H. et al. 3d pulsed chaos lidar system. *Opt. Express* **26**, 12230–12241 (2018).
8. Uchida, A. et al. Fast physical random bit generation with chaotic semiconductor lasers. *Nat. Photonics* **2**, 728–732 (2008).
9. Agrawal, G. P. & Klaus, J. T. Effect of phase-conjugate feedback on semiconductor laser dynamics. *Opt. Lett.* **16**, 1325–1327 (1991).
10. Van Tartwijk, G., Van der Linden, H. & Lenstra, D. Theory of a diode laser with phase-conjugate feedback. *Opt. Lett.* **17**, 1590–1592 (1992).
11. van der Graaf, W. A., Pesquera, L. & Lenstra, D. Stability of a diode laser with phase-conjugate feedback. *Opt. Lett.* **23**, 256–258 (1998).
12. Krauskopf, B., Gray, G. R. & Lenstra, D. Semiconductor laser with phase-conjugate feedback: Dynamics and bifurcations. *Phys. Rev. E* **58**, 7190 (1998).
13. Van der Graaf, W., Pesquera, L. & Lenstra, D. Stability and noise properties of diode lasers with phase-conjugate feedback. *IEEE J. Quant. Electr.* **37**, 562–573 (2001).
14. Erneux, T., Gavrielides, A., Green, K. & Krauskopf, B. External cavity modes of semiconductor lasers with phase-conjugate feedback. *Phys. Rev. E* **68**, 066205 (2003).
15. Dal Bosco, A. K., Wolfersberger, D. & Sciamanna, M. Delay-induced deterministic resonance of chaotic dynamics. *Europhys. Lett.* **101**, 24001 (2013).
16. Mercier, É., Wolfersberger, D. & Sciamanna, M. High-frequency chaotic dynamics enabled by optical phase-conjugation. *Sci. Rep.* **6**, 1–6 (2016).
17. Bouchez, G., Uy, C.-H., Macias, B., Wolfersberger, D. & Sciamanna, M. Wideband chaos from a laser diode with phase-conjugate feedback. *Opt. Lett.* **44**, 975 (2019).
18. Malica, T., Bouche, G., Wolfersberger, D. & Sciamanna, M. Spatiotemporal complexity of chaos in a phase-conjugate feedback laser system. *Opt. Lett.* **45**, 819–822 (2020).
19. Langley, L. & Shore, K. Effect of phase-conjugate optical feedback on the intensity noise in laser diodes. *Opt. Lett.* **18**, 1432–1434 (1993).
20. Green, K. & Krauskopf, B. Bifurcation analysis of a semiconductor laser subject to non-instantaneous phase-conjugate feedback. *Opt. Commun.* **231**, 383–393 (2004).
21. Dal Bosco, A. K., Wolfersberger, D. & Sciamanna, M. Super-harmonic self-pulsations from a time-delayed phase-conjugate optical system. *Appl. Phys. Lett.* **105**, 081101 (2014).
22. Lawrence, J. & Kane, D. Contrasting conventional optical and phase-conjugate feedback in laser diodes. *Phys. Rev. A* **63**, 033805 (2001).
23. Malica, T., Bouchez, G., Wolfersberger, D. & Sciamanna, M. Evolution of the spatiotemporal complexity in a phase-conjugate feedback laser system. in *Semiconductor Lasers and Laser Dynamics IX*, vol. 11356, 113560Z (International Society for Optics and Photonics, 2020).
24. Rontani, D., Mercier, E., Wolfersberger, D. & Sciamanna, M. Enhanced complexity of optical chaos in a laser diode with phase-conjugate feedback. *Opt. Lett.* **41**, 4637 (2016).
25. Zhao, A. et al. Wideband complex-enhanced chaos generation using a semiconductor laser subject to delay-interfered self-phase-modulated feedback. *Opt. Express* **27**, 12336–12348 (2019).
26. Qiao, L. et al. Generation of flat wideband chaos based on mutual injection of semiconductor lasers. *Opt. Lett.* **44**, 5394–5397 (2019).
27. Schires, K., Gomez, S., Gallet, A., Duan, G.-H. & Grillot, F. Passive chaos bandwidth enhancement under dual-optical feedback with hybrid iii–v/si dfb laser. *IEEE J. Select. Top. Quant. Electr.* **23**, 1–9 (2017).
28. Soriano, M. C., Zunino, L., Rosso, O. A., Fischer, I. & Mirasso, C. R. Time scales of a chaotic semiconductor laser with optical feedback under the lens of a permutation information analysis. *IEEE J. Quant. Electr.* **47**, 252–261 (2011).
29. Huyet, G. et al. Dynamics of a semiconductor laser with optical feedback. *Phys. Rev. A* **60**, 1534 (1999).
30. Huyet, G. et al. Low frequency fluctuations and multimode operation of a semiconductor laser with optical feedback. *Opt. Commun.* **149**, 341–347 (1998).
31. Heil, T., Fischer, I., Elsäßer, W. & Gavrielides, A. Dynamics of semiconductor lasers subject to delayed optical feedback: the short cavity regime. *Phys. Rev. Lett.* **87**, 243901 (2001).
32. Tabaka, A., Panajotov, K., Veretennicoff, I. & Sciamanna, M. Bifurcation study of regular pulse packages in laser diodes subject to optical feedback. *Phys. Rev. E* **70**, 036211 (2004).
33. Virte, M., Dal Bosco, A. K., Wolfersberger, D. & Sciamanna, M. Chaos crisis and bistability of self-pulsing dynamics in a laser diode with phase-conjugate feedback. *Phys. Rev. A* **84**, 043836 (2011).
34. Mercier, É., Wolfersberger, D. & Sciamanna, M. Bifurcation to chaotic low-frequency fluctuations in a laser diode with phase-conjugate feedback. *Opt. Lett.* **39**, 4021–4024 (2014).
35. Feinberg, J. Self-pumped, continuous-wave phase conjugator using internal reflection. in *Landmark Papers On Photorefractive Nonlinear Optics*, 315–317 (World Scientific, 1995).
36. Bandt, C. & Pompe, B. Permutation entropy: a natural complexity measure for time series. *Phys. Rev. Lett.,* **88**, 174102 (2002).
37. Riedl, M., Müller, A. & Wessel, N. Practical considerations of permutation entropy. *Eur. Phys. J. Special Top.* **222**, 249–262 (2013).
38. Liu, H., Ren, B., Zhao, Q. & Li, N. Characterizing the optical chaos in a special type of small networks of semiconductor lasers using permutation entropy. *Opt. Commun.* **359**, 79–84 (2016).
39. Zanin, M., Zunino, L., Rosso, O. A. & Papo, D. Permutation entropy and its main biomedical and econophysics applications: a review. *Entropy* **14**, 1553–1577 (2012).
40. Zunino, L., Zanin, M., Tabak, B. M., Pérez, D. G. & Rosso, O. A. Forbidden patterns, permutation entropy and stock market inefficiency. *Physica A: Statistical Mechanics and its Applications* **388**, 2854–2864 (2009).
41. Benítez, R., Bolós, V. & Ramírez, M. A wavelet-based tool for studying non-periodicity. *Computers Math. Appl.* **60**, 634–641 (2010).
42. Bazhenov, V., Pogorelova, O. & Postnikova, T. Intermittent transition to chaos in vibroimpact system. *Appl. Math. Nonlinear Sci.* **3**, 475–486 (2018).
43. Koronovskii, A. & Khramov, A. An effective wavelet analysis of the transition to chaos via intermittency. *Tech. Phys. Lett.* **27**, 1–5 (2001).
44. Lin, F. & Liu, J. Nonlinear dynamical characteristics of an optically injected semiconductor laser subject to optoelectronic feedback. *Opt. Commun.* **221**, 173–180 (2003).
45. Bouchez, G., Malica, T., Wolfersberger, D. & Sciamanna, M. Optimized properties of chaos from a laser diode. *Phys. Rev. E* **103**, 042207 (2021).
46. Weicker, L., Erneux, T., Wolfersberger, D. & Sciamanna, M. Laser diode nonlinear dynamics from a filtered phase-conjugate optical feedback. *Phys. Rev. E* **92**, 022906 (2015).
47. DeTienne, D. H., Gray, G. R., Agrawal, G. P. & Lenstra, D. Semiconductor laser dynamics for feedback from a finite-penetration-depth phase-conjugate mirror. *IEEE J. Quant. Electr.* **33**, 838–844 (1997).

Acknowledgements

Author contributions

T.M. and M.S. conceived the idea of interpretating the experimental data in the presented context. T.M. developed the methodology, calculated, and performed the presented analyses. The experimental setup and the theoretical model was designed and developed by G.B., D.W., and M.S. The final draft was written by T.M. with contributions from M.S., D.W., and G.B.

Competing interests

The authors declare no competing interests.

Additional information